

## PHASE MASKS IN ASTRONOMY: FROM THE MACH-ZEHNDER INTERFEROMETER TO CORONOGRAPHS

Kjetil Dohlen<sup>1</sup>

**Abstract.** Phase masks have numerous applications in astronomical optics, in particular related to two themes: coronagraphy for detection and analysis of extrasolar planets or circumstellar disks, and wavefront analysis for extremely precise adaptive optics systems or cophasing of segmented mirrors. I review some of the literature concerning phase masks and attempt to bridge the gap between two instrumental systems in which they are often found: the Mach-Zehnder interferometer and the coronagraph.

### 1 Introduction

Zernike (1934) introduced phase masks into astronomical optics when he proposed the use of a phase-shifting spot to replace Foucault's classical knife edge for testing of optical surfaces. He showed that this allowed photometric measurement of surface phase errors rather than surface slope errors, and, as a bi-product of this work, he found it convenient to introduce a certain series of polynomials, facilitating the analysis of his surface maps. Zernike's name is forever associated with the polynomials rather than with the phase mask. A similar procedure was later proposed by Smartt & Strong (1972).

Angel (1994) proposed to use an adaptation of the Zernike test based on a Mach-Zehnder interferometer as wavefront sensor for high-performance adaptive optics systems. The Mach-Zehnder interferometer has the advantage over the Michelson interferometer of separating the output beam from the input beam, hence providing one-way traffic between separation and recombination of the beams, see Fig. 1. Letting the beam go through a focus within the interferometer, beam modification by spatial filtering is possible, and Angel's proposition

---

<sup>1</sup> Laboratoire d'Astrophysique de Marseille  
2 place Leverrier, 13248 Marseille Cedex 4, FRANCE  
Tel : + 33 (0) 4 95 04 41 24, Fax : + 33 (0) 4 91 62 11 90  
e-mail : kjetil.dohlen@oamp.fr

was to filter the beam in one arm by a pin-hole the size of an Airy disk, thus creating a spherical reference wave.

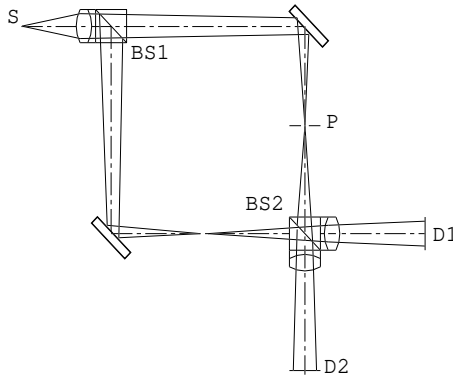


**Fig. 1.** Diagram of the Mach-Zehnder interferometer as a wavefront sensor with a pinhole (P) in one of the arms in an image of the source (S).

More recently, the same basic principle has been proposed as a phasing sensor for extremely large telescopes (Dohlen *et al.* 1998). The pinhole is here larger, roughly the size of the atmospheric seeing disk, in order to minimize the effect of atmospheric turbulence on the estimation of inter-segment phase errors in segmented mirrors.

Another astronomical optical component resembling Zernike’s test is the Roddier phase mask coronagraph (Roddier & Roddier 1997), providing interferometric extinction of starlight in the hope of achieving direct imagery of extrasolar planets. But while Zernike’s dot was adjusted to produce a roughly  $90^\circ$  phase shift, Roddier’s dot needs to produce a very precise  $180^\circ$  phase shift. Also, where the former was fairly tolerant to dot size, the latter required a diameter equal to a precise fraction of the Airy disk. Of course, as the dot’s phase shifting capacity is chromatically dependent unless composed of a stack of dielectric materials, and since the Airy disk’s diameter also varies with wavelength, the required nulling can only be achieved within very narrow wavelength bands.

We have recently proposed a generalization of Roddier’s coronagraph where the dot is surrounded by a ring with a different phase shift (Soummer *et al.* 2003). As wavelength increases, the phase lag decreases both for the dot and the ring, but since at the same time the fractions of the Airy disk covered also vary, complex vector analysis shows that the total transmission remains close to zero over a wide wavelength range, making this component an interesting option for wide-band stellar coronagraphy.

In this paper we describe fundamentals and practical aspects of these instruments, illustrated by simulations. In Section 2, we describe the major functionalities of the Mach-Zehnder interferometer in its astronomical sensor applications, and in Section 3 we present a vector-based discussion of (circular) phase-mask

coronagraphs. In Section 4 we investigate the equivalence between the Mach-Zehnder interferometer and phase mask coronagraphs and indicate situations in which the use of one or the other may be beneficial from a performance and/or practical implementation point of view.

## 2 The Mach-Zehnder interferometer

The Mach-Zehnder interferometer serves as a base concept for numerous instruments within all fields of optics. Astronomical optics is no exception as illustrated for example by the imaging Fourier transform spectrometer currently under construction for the SPIRE instrument (Swinyard *et al.* 2002) for ESA's 3.5-meter diameter far infrared space telescope Herschel (Pilbratt 2001). We are here concerned with rather different astronomical applications, where the goal is not to analyze the spectral content of the source, but to analyze the shape of the transmitted wavefront in order to correct it adaptively or actively.

### 2.1 Wavefront sensor for extreme AO

In the concept proposed by Angel (1994), the wavefront is split into two equal parts just before going through a focus, see Figure 1. In one of the arms, a pinhole placed in the focus acts as a spatial filter and provides a spherical reference wavefront. At the output beamsplitter, the original wavefront interferes with the reference wavefront, and fringes representing the wavefront defects are observed in a pupil image. Since the Mach-Zehnder interferometer has two accessible outputs, containing complementary fringe patterns, two images are formed; the difference between these images is referred to as the Mach-Zehnder signal.

When the optical path difference (OPD) between the arms is adjusted to zero, the signal is proportional to the cosine of the wavefront errors, ie, for small errors, the signal is related to the square of the wavefront error. If, however, the OPD is set to  $\lambda/4$ , then the signal is proportional to the sine of the wavefront error, hence linear for small errors. Reconstruction-free wavefront sensing is therefore possible in closed loop operation, if a one-to-one relationship exists between the pixels of the signal and the deformable mirror actuators. This is illustrated in Fig. 2 where the phase screen representing an atmospheric wavefront of  $0.1\lambda$  rms error is compared with the measured signal. Assuming a linear approximation for the sine, the wavefront estimation error is in this case  $0.025\lambda$ , but in closed loop, this residual is rapidly reduced, as illustrated in Fig. 3, showing the PSF for the first three steps of simulated closed loop operation assuming linear reconstruction and ignoring all noise sources.

Stahl & Sandler 1995 investigated the use of this type of wavefront sensor in their study of an adaptive system for exoplanet detection consisting of an 11 000-actuator DM controlled at a 2 kHz update rate. They concluded that, while instrumentally challenging, Jupiter-like planet could be detected around nearby stars, and that a survey of 30 stars within 10 pc could be reasonably foreseen using the 6.5m MMT.

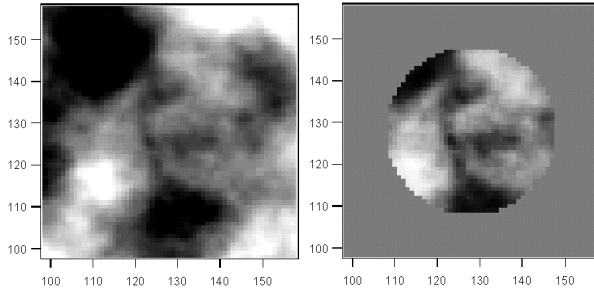


**Fig. 2.** Phase screen representing a wavefront error of  $0.1\lambda$  rms (left) and the measured Mach-Zehnder signal for an OPD between the two arms of  $\lambda/4$  (right).

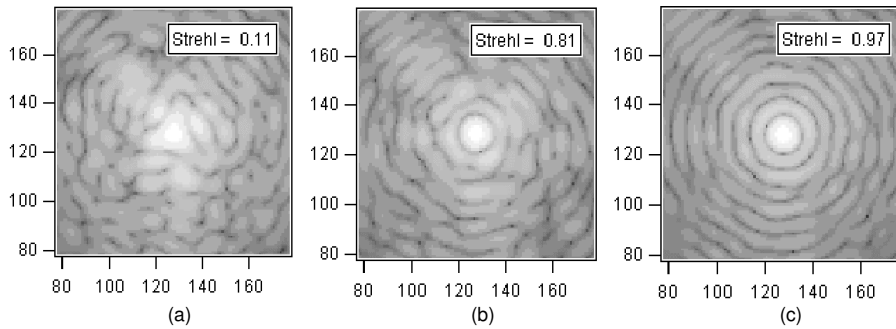


**Fig. 3.** PSF corresponding to the first three steps of simulated closed loop operation of a Mach-Zehnder-based adaptive optics system, assuming linear reconstruction and ignoring all noise sources. Intensity is coded logarithmically.

Laboratory demonstrations of very fine-scale wavefront retrieval has been achieved (Langlois *et al.* 2001), where the Mach-Zehnder signal was captured using two  $128 \times 128$  pixel CMOS detector arrays and pixel-by-pixel coupled with a liquid crystal (LC) spatial phase modulator. While alignment between detectors and LC limited the performance, a residual phase error smaller than  $1/5$  of the  $\lambda/18$  initial wavefront error was reported.

This method works fine for small wavefront errors, but it is less adapted to errors exceeding  $\lambda/4$  ( $\pi/2$  radians), as is generally the case for the uncorrected atmosphere. Three options allow to overcome this problem: Pre-correction using classical low-order AO, rapid phase shifting using a piezo actuator to vary the OPD between the Mach-Zehnder arms, and boot-strapping by actively varying the pinhole size. The first option is conceptually simple and allows for upgrading of existing AO systems, but the total system becomes rather complex. The second option, assumed by Stahl & Sandler (1995) requires extremely high measurement rates to allow sequential phase stepping in the presence of an evolving phase screen. Also, the flux transmitted by the pinhole is very small compared to the total

wavefront flux, giving a low-contrast interferogram.

The boot-strapping method, mentioned by Angel (1994), is certainly the most elegant option, although the fabrication of a variable-size precision pinhole may be a challenge. Increasing the pinhole, which acts as a spatial low-pass filter, shifts the cut-off frequency upwards. After recombination, the resulting wavefront represents the difference between the filtered and unfiltered wavefronts, and so the total operation can be seen as high-pass filtering, transmitting only the wavefront components beyond the cut-off frequency given by the pin-hole size. For a pinhole size corresponding to the seeing disk, the remaining aberrations can be expected to represent approximately 1 radian, appropriate for the reconstruction-free approach. Once closed loop operation has been established, the pinhole size can gradually be reduced until the diffraction limit is reached. Figure 4 shows the starting point PSF, an intermediate, and the final corrected PSF for a very simple simulation using a fixed phase screen whose initial wavefront rms was  $\lambda/2$  and a dynamically variable pinhole diameter.

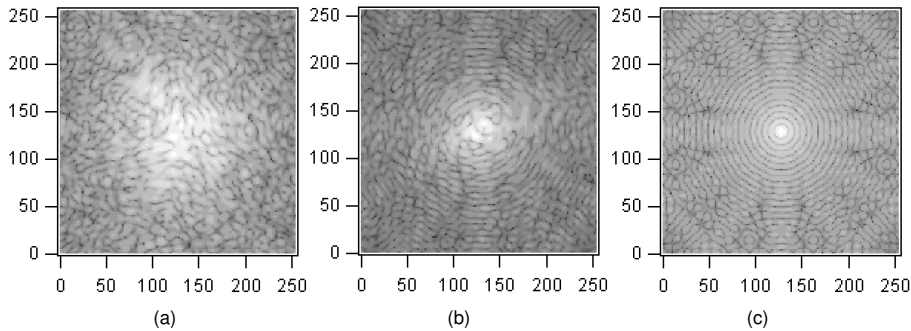


**Fig. 4.** PSFs representing the starting point (a), an intermediate step (b), and the final result (c) for a boot-strapped Mach-Zehnder wavefront sensor whose pin-hole diameter varies dynamically. Intensity is coded logarithmically.

## 2.2 Cophasing sensor

The use of a Mach-Zehnder with a large pinhole has also been proposed in the context of measuring inter-segment phase steps in extremely large telescopes (ELTs) (Dohlen *et al.* 1998). All current ELT projects depend on the use of segmented primary mirrors, and some projects (Dierickx & Gilmozzi 2000) also rely on a (flat) segmented secondary mirror. While the basic technologies required for segmented telescopes have been demonstrated on the Keck telescopes, ELTs of diameters from 30 to 100 m represent quantum leaps of one to two orders of magnitude in segmentation complexity compared with current 10-m technology.

Calibration of the phasing system remains an important issue, and it is not clear that the proven Keck technology, based on accurate positioning of micro pupils at the intersections between segments, is transposable to the ELT case. A

general issue concerns the accuracy required in micro pupil mask fabrication and alignment, a more specific issue, related to the use of two segmented mirrors, is that of separating the two segmentation patterns. The latter point is aggravated by the fact that guide stars used for phasing measurements can be located anywhere within the technical field of view (FOV) of the telescope. As the guide star moves across the FOV, the segmentation patterns move one with respect to the other, making the use of a fixed micro pupil mask impossible.

An alternative approach consists of coding the phase errors as intensity variations in a pupil image projected onto a detector array. This allows direct pixel-by-pixel processing and avoids the use of a pupil mask. Several methods have been proposed to achieve intensity coding of the phase errors, including the use of pupil defocus, first proposed and demonstrated by Chanan *et al.* 1999 for the Keck telescope and later described theoretically in terms of wave front curvature by Cuevas *et al.* (2000) in analogy with curvature sensing for adaptive optics (Roddier 1990). More recently, it has been shown that the pyramid wave front sensor—a modernized version of the Foucault knife-edge test, developed for adaptive optics—is also sensitive to segment dephasing (Esposito *et al.* 2003). Use of the Mach-Zehnder interferometer was first proposed by Dohlen *et al.* (1998), and described in its present form by Montoya Martinez *et al.* (2002).

As in the bootstrapping procedure described above, the low frequencies of the atmospheric errors are removed by using a pinhole approximately the size of the seeing disk. This also removes the low-frequency components of the segment phase errors, but since the frequency content of a step function is very wide, sufficient information remains. As seen in Fig. 5, showing the signal profile for different piston values in the absence of atmospheric turbulence, a brightening on one side and a darkening on the other side of the edge appears, with a sharp transition between dark and bright. The dark-bright amplitude is proportional to the sine of the piston step, with a peak at  $\pi/2$  and falling to zero at  $\pi$ . The signal is perfectly symmetrical, and identical for a pistons of  $\pi/2 \pm \delta$ .

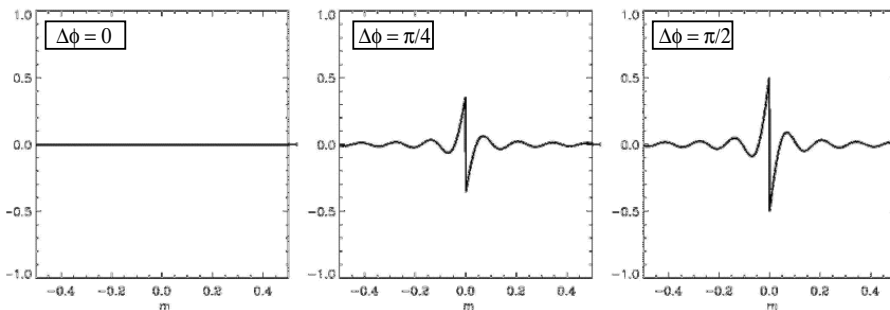


**Fig. 5.** Mach-Zehnder signal in the absence of atmosphere for piston values of 0 (left),  $\pi/4$  (middle), and  $\pi/2$  (right).

Since the high spatial frequency atmospheric phase residuals vary with time,

they tend to disappear in long-exposure, see Fig. 6. Optimal performance requires exposure times of typically a few seconds.

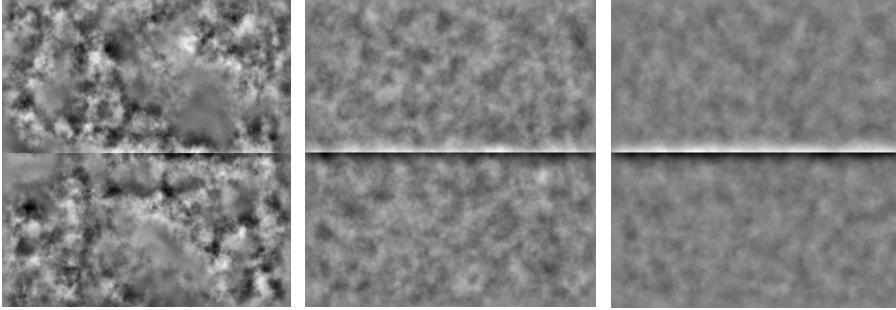


**Fig. 6.** Simulated Mach-Zehnder signal for different exposure times, representing one (left), 25 (middle) and 100 (right) phase screens.

Extracting the piston information from the Mach-Zehnder signal can be done by estimating the dark-to-bright amplitude, or as the difference between the integral of the signal between the edge and the first zero crossing on either side of the edge. Fig. 7 shows the result of the integral method for a piston of  $\pi/2$  as a function of pinhole size in the absence of atmospheric errors (continuous line) and for three different atmospheres. While the signal amplitude stays constant whatever the pinhole, the width of the signal, and hence the integral, diminishes as the pinhole grows. In the presence of atmospheric errors, the signal disappears for small pinholes, goes through a maximum close to the seeing disc diameter (indicated by vertical bars), and joins the ideal curve for pinholes larger than about twice the seeing disc diameter.

The presence of gaps and turned-down edges, as well as practical problems related to signal detection involving pixel convolution and sampling, affects the signal significantly. In particular, effects of turned-down edges such as the zero-piston residual signal, are amplified as the pinhole size grows, indicating the use of small pinholes. Optimal performance is in practice obtained by using a pinhole approximately the size of the median-seeing seeing disk associated with an iterative alignment procedure. While the use of a small pinhole results in an uncertainty in the exact piston amplitude because the seeing parameter is variable and *a priori* unknown, it minimizes the zero-offset problem induced by turned-down edges. Simulations indicate that an error below 20nm after a few iterations will be achieved.

### 3 Phase mask coronagraphs

While early stellar coronagraphy for imaging of faint objects close to bright stars were simple adaptations of the Lyot solar coronagraph, the phase mask coronagraph proposed by Roddier & Roddier (1997) was the first to utilize the spatial

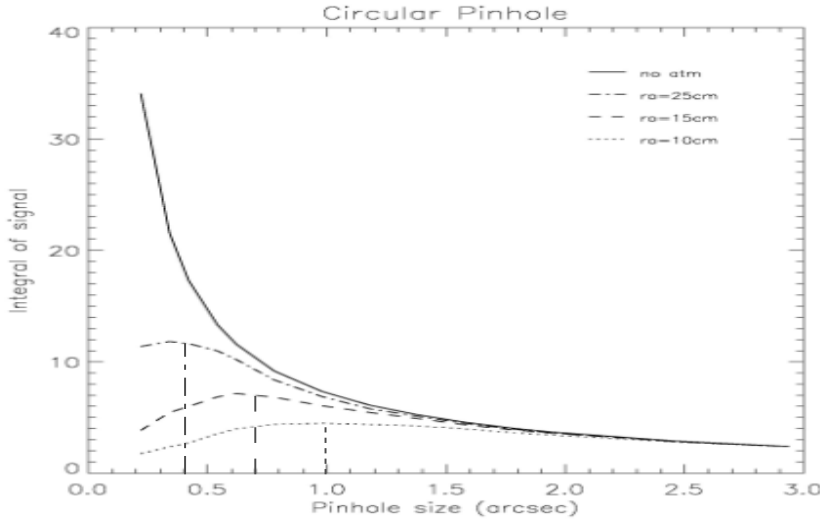


**Fig. 7.** Calibration curves for the Mach-Zehnder phasing sensor in the absence of atmosphere (solid line) and for different atmospheric conditions. Vertical bars indicate the seeing disk dimension.

coherence of stellar sources and to obtain nulling by interferometric extinction. Instead of blocking the stellar flux, part of it was phase shifted by  $180^\circ$  in order to interfere destructively with the remaining flux. A simple illustration of this technique based on Fourier theory can be made by considering the center of the pupil, where the value of the complex electric field is equal to the integral of the image-plane electric field. In order to bring the field at the pupil center to zero, the size of the phase mask must be adjusted so that the integral within the phase mask exactly matches the integral outside the mask, see Fig. 8 (b). Elsewhere in the pupil, the nulling is not perfect, and a careful optimization of the mask diameter will be necessary to select the optimum nulling zone. However, perfect nulling can be achieved by this method if the entrance pupil is apodized (Guyon & Roddier 2000, Aime *et al.* 2002).

The Lyot stellar coronagraph can also be used in a nulling mode by adjusting the diameter of the (opaque) mask such that the integral of the transmitted flux is zero, see Fig. 8 (a). Again, apodization is required for optimal nulling (Aime *et al.* 2002). This concept is referred to as the Prolate Apodized Lyot Coronagraph (PALC).

Both the Roddier and Lyot nulling coronagraph are chromatic, with optimal performance at a single wavelength. At other wavelengths, the size of the diffraction spot changes, and so the value of the integrals. Also, for the Roddier concept, the optical path through the phase mask changes unless built up as an achromatic combination of several materials. Soummer *et al.* (2003) has proposed an achro-

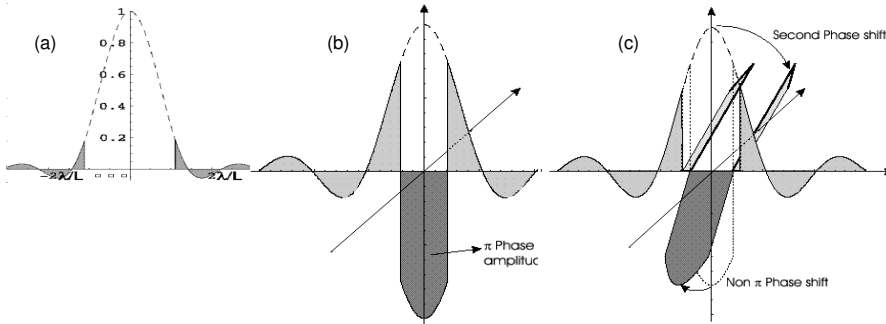


**Fig. 8.** Illustration of the principle of interferential nulling phase mask coronagraphs: Lyot (a), Roddier (b) and dual zone (c). In each case, the integral of the complex field transmitted through the mask is zero.

matized, dual zone (DZ) version of the phase-mask coronagraph, where the phase shifting mask is surrounded by a phase shifting annulus, see Fig. 8 (c). An infinite number of solutions can be found for which the complex integral of the field transmitted by this mask is zero, providing zero amplitude at the center of the exit pupil at a given wavelength. By fairly simple analysis, one can also show that solutions exist which give zero integral at two different wavelengths, as illustrated in Fig. 9 in terms of complex vector summation. Optimal nulling over the entire pupil and for a given band is found by numerical least squares optimization of the diameter of each mask zone and their optical thicknesses as well as apodization parameters. It is interesting to note that this concept is improved by applying complex apodization, involving the variation of phase as well as transmission across the pupil. In practice, phase apodization is achieved simply by introducing a slight defocus of the coronagraph mask.

#### 4 Mach-Zehnder–coronagraph equivalences

The Mach-Zehnder interferometer combined with a pinhole and a phase shifter as described above is similar to a phase mask coronagraph. In fact, each Mach-Zehnder output has an equivalent coronagraphic phase mask of complex transmission  $\mathbf{M}_{\text{coro}} = \mathbf{M}_1 \pm \mathbf{M}_2$ , where  $\mathbf{M}_1$  and  $\mathbf{M}_2$  are complex transmissions of the focal plane mask in each Mach-Zehnder arm and the choice of sign corresponds to the choice of output. In the MZ systems we have considered so far for wavefront sensing,  $\mathbf{M}_1$  has unit transmission everywhere (transparent) and  $\mathbf{M}_2$  has unit transmission within the pinhole and zero outside. The optical path difference introduced between the arms is accounted for by adding a phase angle to one of the mask functions.

A possibility offered by this equivalence is to replace the interferometer in the phasing sensor by its coronagraphic equivalence. Although the advantage of

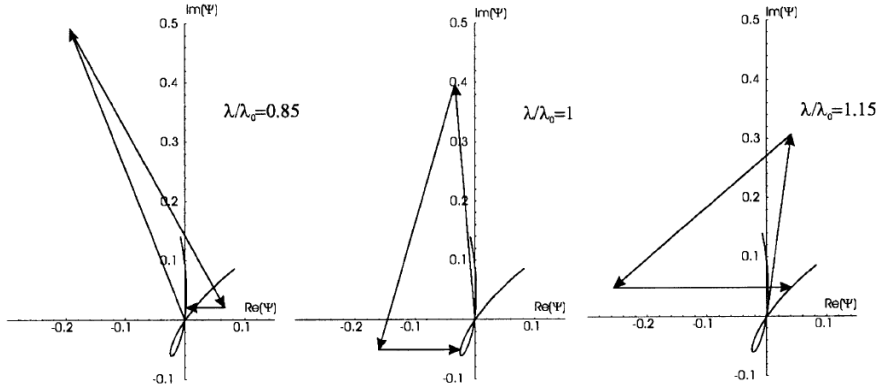


**Fig. 9.** Illustration of the three-vector addition in the complex plane. The resulting vector describes a  $\gamma$ -like curve as the wavelength varies across the band.

having access to two outputs in terms of signal cleanliness etc. is lost, this clearly would simplify the opto-mechanical design of the system. Strictly speaking, the coronagraphic equivalence of the proposed Mach-Zehnder phasing sensor has a  $45^\circ$  phase-shifting spot with twice the transmission of its surroundings. Studying different phase and transmission distributions, it has been found that an equal-transmission phase mask with a  $45^\circ$  phase shifting dot gives an optimally symmetrical signal. Fig. 10 shows the signal profile obtained in this case for piston steps of  $0$ ,  $\pi/2$  and  $\pi$ . The two leftmost profiles can be compared with the left and right profiles of Fig. 5, respectively. A slight asymmetry develops as the piston step grows, and at piston of  $\pi$ , where the “classical” Mach-Zehnder signal is zero, a small residual is present. This can actually be seen as an advantage, allowing an increase of the calibration range.

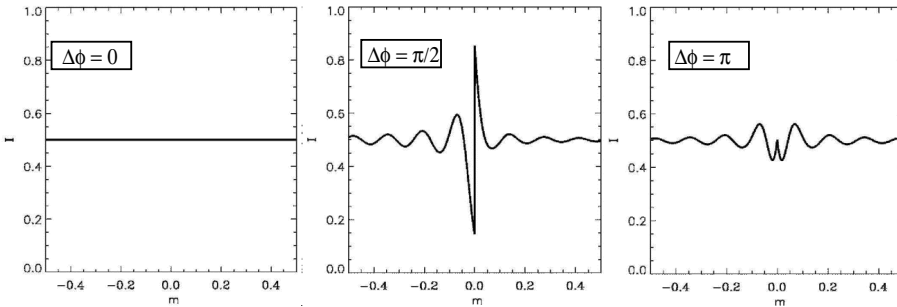


**Fig. 10.** Signal profiles for the coronagraphic version of the Mach-Zehnder phasing sensor in the absence of atmosphere and for piston values of  $0$  (left),  $\pi/2$  (middle), and  $\pi$  (right). The mask has unit transmission and a  $45^{\text{circ}}$  dephasing.

On the other hand, interferometric equivalences of coronagraphic devices may offer access to a larger design space than the simple phase mask approach. Also, the concept can be generalized by using transmission phase masks rather than pinholes, and different masks in each arm. Playing with mask material (dispersion, absorption, etc) and dimensions, a large number of variables are available, allowing optimization of performance according to applications and requirements. In particular, this could provide coronagraphs of the dual zone type while avoiding the difficulty of manufacturing the dual zone mask.

Other interesting hybrids involving coronagraphs and Mach-Zehnder interferometers are being published at the time of this writing by Codona & Angel (2004) and Labeyrie (2004), both of which are based on active interferometric speckle suppression (“active halo nulling”). The star image is focussed onto the first beam splitter (BS1 in Fig. 1), which is replaced by a mirror with a pinhole approximately the size of the Airy disk. This acts as a Lyot-type coronagraph for the reflected beam, which, in conjunction with appropriate apodization, provides an image riddled of the Airy pattern but polluted by a residual speckle halo. The transmitted beam, containing the major part of the spatially coherent starlight, is modified, either using phase and amplitude spatial light modulators (Codona & Angel 2004) or a real-time generated holographic optical element (Labeyrie 2004), and made to interfere, destructively, with the coronagraphic beam at the output beam splitter. The value of this approach is reported to be the relaxed precision required for the wavefront control of the reference beam, greatly reduced compared with the requirements for the pre-coronagraph wavefront control.

## 5 Conclusion

Phase masks are used in various branches of astronomical optics, in particular for wavefront characterization and coronagraphic nulling. We have reviewed different concepts and applications of phase masks both in their coronagraphic form and in the form of Mach-Zehnder interferometers. While phase mask coronagraphs will be important in the search and characterization of extra-solar planets and circumstellar disks, the Mach-Zehnder wavefront sensor will certainly have an important role to play in future high-performance adaptive optics systems and as a phasing sensor for future generations of large segmented telescopes.

The equivalence between coronagraphic and interferometric phase masks has been established, and possible advantages of using one or the other in terms of performance and feasibility have been pointed out. Finally, extremely interesting developments of Mach-Zehnder–coronagraph hybrids using active interferometric speckle suppression have been reported.

**Acknowledgements** I am grateful to Luzma Montoya Martinez for providing illustrations from her work on the Mach-Zehnder phasing sensor, and to Antoine Labeyrie for inviting me to make this talk as a *College de France* seminar.

## References

- Aime, C., Soummer, R. 2002, in *Astronomy with High Contrast Imaging: from planetary systems to active galactic nuclei*, C. Aime and R. Soummer, Eds (EAS Publication Series)
- Angle, R. 1994, *Nature* 368, 203
- Chanan, G., Troy, M. & Sirko, E. 1999, *ApOpt* 38, 704
- Codona, J. L., Angel, R. 2004, *ApJ* 604, L117,
- Cuevas, S., Orlov, V.G., Garfias, F., Voitsekhovich, V.V., Sanchez, L.J. 2000, *Proc. SPIE* 4003, 291
- Dierickx, P., Gilmozzi, R. 2000, *Proc. SPIE* 4004, 290
- Dohlen, K., Decortiat, R., Fresneau, F., Lanzoni, P. 1998, *Proc. SPIE* 3352, 551
- Esposito, S., Pinna, E., Tozzi, A., Stefanini, P., Devaney, N. 2003, *Proc. SPIE* 5169, 72
- Guyon, O., Roddier, F. 2000, *Proc. SPIE* 4006, 377
- Labeyrie, A. 2004, these proceedings
- Langlois, M., Angel, R., Lloyd-Hart, M., Wildi, F., Love, G., Naumov, A. 2001, in *Beyond Conventional Adaptive Optics*, E. Vernet, R. Ragazzoni, S. Esposito, N. Hubin Eds. (ESO Conference and Workshop Proceedings No. 58), 113
- Montoya Martinez, L., Yaitskova, N., Dierickx, P., Dohlen, K. 2002, *Proc. SPIE* 4840, 564
- Pilbratt, G.L. 2001, in *"The promise of the Herschel Space Observatory"*, ed. G.L.Pilbratt, J.Cernicharo, A.M. Heras, T. Prusti, & R. Harris (ESA SP-460), p. 13
- Roddier, F. 1990, *ApOpt* 29, 1402
- Roddier, F., Roddier, C. 1997, *PASP* 109, 815
- Smartt, R.N., Strong, J. 1972, *J. Opt. Soc. Am.* 62, 737
- Soummer, R., Dohlen, K., Aime, C. 2003, *A& A* 403, 369
- Stahl, S.M., Sandler, D.G. 1995, *ApJ* 454, L153
- Swinyard, B. M., Dohlen, K., Ferand, D., Baluteau, J.-P., Pouliquen, D., Dargent, P., Michel, G., Martignac, J., Ade, P.A.R., Hargrave, P.C., Griffin, M. J., Jennings, D.E., & Caldwell, M.E. 2002, *Proc. SPIE* 4850, 698
- Zernike, F. 1934, *F. Mon. Not. R. astr. soc.* 94, 377